Proceedings of FUELCELL2006
The 4th International Conference on FUEL CELL SCIENCE, ENGINEERING and TECHNOLOGY
June 19-21, 2006, Irvine, CA

FUELCELL2006-97106

SHAPE OPTIMIZATION OF FUEL CELL MOLDED-ON GASKETS FOR ROBUST SEALING

Andreas Vlahinos[1], Kenneth Kelly[2], Kevin Mease[3], Jim Stathopoulos[3]

[1]Advanced Engineering Solutions LLC, Castle Rock, CO, 80108, USA, andreas@aes.nu
[2]National Renewable Energy Laboratory, Golden, CO, 80401, USA kenneth_kelly@nrel.gov
[3]Plug Power, Inc., Latham, NY, 12110, USA, kevin_mease@plugpower.com
[3]Plug Power, Inc., Latham, NY, 12110, USA, dimitrios.stathopoulos@ge.com

ABSTRACT

In typical Proton Exchange Membrane fuel cells, a compressed gasket provides a sealing barrier between cell and cooler bipolar plate interfaces. The gasket initially bears the entire bolt load, and its resisting reaction load depends on the cross-sectional shape of the gasket, bipolar plate's groove depth, and the hyperelastic properties of the gasket material.

A nonlinear, finite element analysis (FEA) model with various hyperelastic material models, large deformations, and contact was used to evaluate the load-gap curves. The deformed shapes and the distributions of stress, strain, and deflections are presented. Mooney-Rivlin and Arruda-Boyce hyperelastic material models were used, and a comparison of load–gap curves is shown. A process is presented that couples the computer-aided design geometry with the nonlinear FEA model that was used to determine the gasket's cross-sectional shape, which achieves the desired reaction load for a given gap.

INTRODUCTION

The main objective of this research effort is to determine alternative gasket and groove configurations of the cooler and cell interfaces to provide robust sealing. In an effort to obtain optimum robust design that is insensitive to variations in noise parameters—such as manufacturing tolerances, material properties, process capability, tooling wear, etc.—a probabilistic FEA analysis was performed. The gasket profile, the gasket groove depth, the recessed opposing plate's pocket groove depth, and the interface gap were considered as randomly varying parameters with given mean and standard deviation. The response surface of the contact force per unit length of the gasket was determined in terms of the probabilistic input variables. The sensitivity of each of the input variables on the contact force is presented. The probability density function of the contact force was determined and compared to the various upper and lower specification limits (LSLs) of cell and cooler interfaces. The sigma-quality level for each target is determined, and the methodology for implementing robust design used in this research effort is summarized in a reusable workflow diagram.

NOMENCLATURE

μ	Initial shear modulus of material
λ_m	Limiting chain extensibility (locking stretch)
CAE	Computer-aided engineering
C_{ij}	Components of the right Cauchy-Green deformation tensor
d	Material incompressibility parameter
E_{ij}	Components of the Lagrangian strain tensor
FEA	Finite element analysis
GGD2	Lower gasket groove depth
μ_{GGD2}	Mean value of lower gasket groove depth
σ_{GGD2}	Standard deviation of lower gasket groove depth
GPO1	Gasket profile offset value
μ_{GPO1}	Mean value of gasket profile offset
σ_{GPO1}	Standard deviation of gasket profile offset
IG4	Interface gap between the bipolar plates
I_1	The first deviatoric strain invariant

J_{el} The elastic volume ratio
LSL Lower specification limit
MEA Membrane electrode assembly
PGD3 Upper gasket groove depth
μ_{PGD3} Mean value of upper gasket groove depth
σ_{PGD3} Standard deviation of upper gasket groove depth
S_{ij} Components of the second Piola-Kirchhoff stress tensor
USL Upper specification limit
W Strain energy function per unit undeformed volume

MATERIAL MODELS

In order to evaluate the performance of several topologies a FEA model, linked to the computer-aided design geometry, was generated. The FEA model is highly nonlinear since large deformations, contact and hyperelastic material behavior are present. The cooler plate material model is linear elastic and the gasket material is hyperelastic. A material is said to be hyperelastic if there exists a strain energy density function W which is a scalar function of one of the strain or deformation tensors, whose derivative with respect to a strain component determines the corresponding stress component. This can be expressed by:

$$S_{ij} = \frac{\partial W}{\partial E_{ij}} = 2\frac{\partial W}{C_{ij}}$$

where:
S_{ij} = components of the 2nd Piola-Kirchhoff stress tensor
W = strain energy function per unit undeformed volume
E_{ij} = components of the Lagrangian strain tensor
C_{ij} = components of the right Cauchy-Green deformation tensor

Two hyperelastic material models were implemented: the three-parameter Mooney-Rivlin Material Model and the Arruda-Boyce Material Model.

The form of the strain energy density function for the three parameter Mooney-Rivlin model is:

$$W = c_{10}(I_1 - 3) + c_{01}(I_2 - 3) + c_{11}(I_1 - 3)(I_2 - 3) + \frac{1}{d}(J - 1)$$

where: c_{10}, c_{01}, c_{11} and d are material constants

The form of the strain energy density function for Arruda-Boyce model W can be found by taking a series expansion of the inverse Langevin function to the 5th order [Ref 1]:

$$W = \mu \sum_{i=1}^{5} \frac{C_i}{\lambda_m^{2i-2}} \left(I_1^i - 3^i \right) + \frac{1}{D}\left(\frac{J_{el}^2 - 1}{2} - \ln J_{el} \right)$$

where:
C_1 = 1/2
C_2 = 1/20
C_3 = 11/1050
C_4 = 19/7000
C_5 = 519/673750
μ = initial shear modulus of material
λ_m = the limiting chain extensibility (locking stretch)
d = material incompressibility parameter
I_1 = the first deviatoric strain invariant
J_{el} = the elastic volume ratio = 1 for incompressible materials

Curve fitting of the experimental stress-strain results, provided by the material vendor, was used to extract the material model coefficients.

FINITE ELEMENT MODEL

A plain strain finite element model was generated in order to compute the reaction force per unit length of the gasket. A high quality mesh was generated in order to accommodate all nonlinearities. Figure 1 shows the undeformed mesh for the cooler interface gasket.

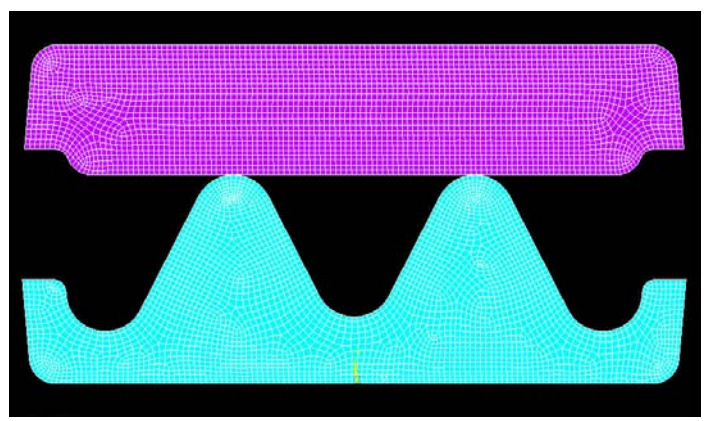

Figure 1 Undeformed Mesh for the Cooler Interface Gasket

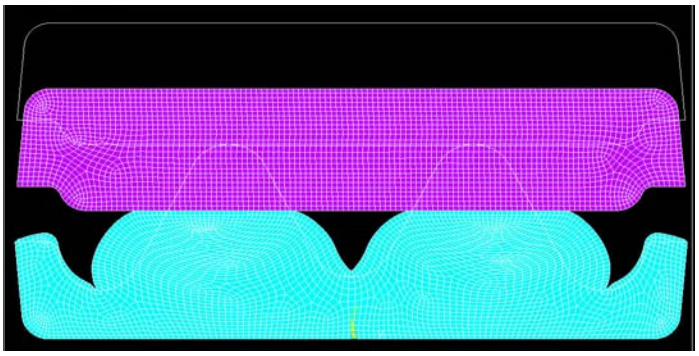

Figure 2 Deformed Shape for the Cooler Interface Gasket

The base of the gasket was restrained against all displacements, and a linearly increasing displacement was imposed on the top of the cooler plate. A contact interface was established between the bottom of the cooler and the top gasket surfaces. The reaction loads were monitored and plotted against the imposed displacement, generating the load versus deflection curves.

A similar model was generated for the gaskets between the anode and cathode. In this case, a gasket-to-gasket contact interface was built in the model, since both plates have a gasket. Figure 3 shows the deformed mesh for the cell interface gaskets. The top gasket's and bottom gasket's material models are hyperelastic. Two hyperelastic material models were also implemented: the Mooney-Rivlin and Arruda-Boyce models.

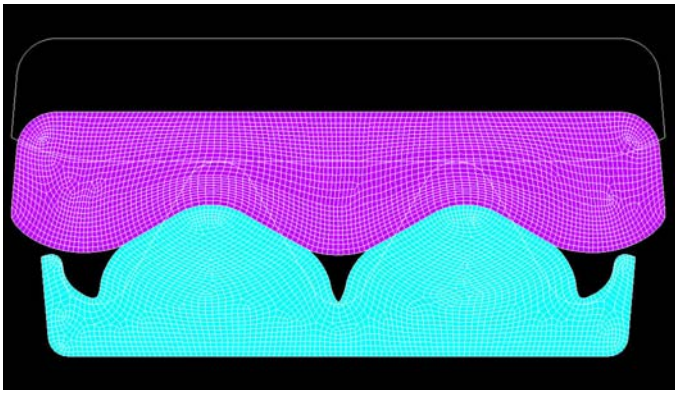

Figure 3 Deformed Shape for the Cell Interface Gasket

A target gasket reaction force of 18 lbs/in at 11.5 mils gap between the bipolar plates was established. If this force is much greater than the target the plates crack, and if this force is much smaller than the target for certain temperature and preload conditions, they don't provide sufficient sealing. Several geometries were simulated in order to obtain the target reaction at the desired gap. The optimum geometry is shown in Figure 1.

Figure 4 shows the optimum cooler interface shape, the vertical displacement distribution, and the contact reaction forces at 10 mils gap. Figure 5 shows the optimum cell interface shape, the vertical displacement distribution, and the contact reaction forces at 10 mils gap. Figure 6 shows the load deflection curves for the final geometry and different material models.

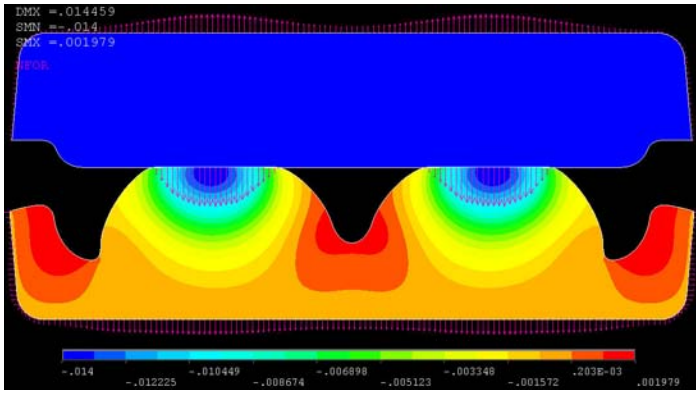

Figure 4 Cooler Interface - Vertical Displacement Distribution and Contact / Reaction Forces at 10 mils Gap

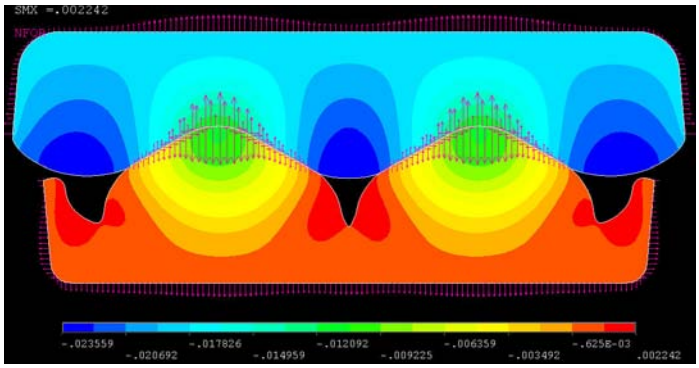

Figure 5 Cell Interface - Vertical Displacement Distribution and Contact / Reaction Forces at 10 mils Gap

Comparison of Mooney-Rivlin and Arruda-Boyce hyperelastic material models shows no difference in the deflected shape and similar load-gap curves. A 6.4% difference on the reaction force at 11.5 mils gap was observed. The reaction at 11.5 mils gap is 17.49 lb/in with the Mooney-Rivlin Material Model and 16.37 lb/in with the Arruda-Boyce Material Model. Figure 6 shows the load-deflection curves for the Mooney-Rivlin and Arruda-Boyce material models. The Arruda-Boyce model is recommended for very large, tensile strains greater than 200%.

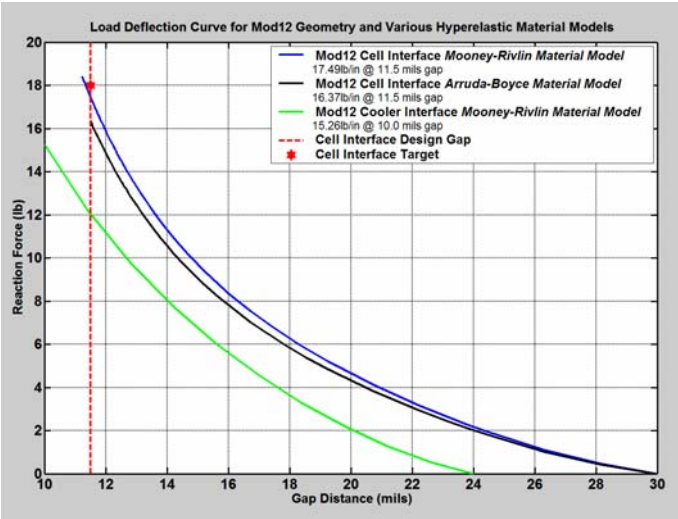

Figure 6 Load-Deflection Curves for Mooney-Rivlin and Arruda-Boyce Material Models

ROBUSTNESS ASSESSMENT

The optimum shape determined is considered the nominal shape. Due to manufacturing variations—such as tolerances, mold wear, temperature, material consistency, etc.—a variation from the nominal shape can be observed. Figure 7 shows the range of minimum and maximum shape variation.

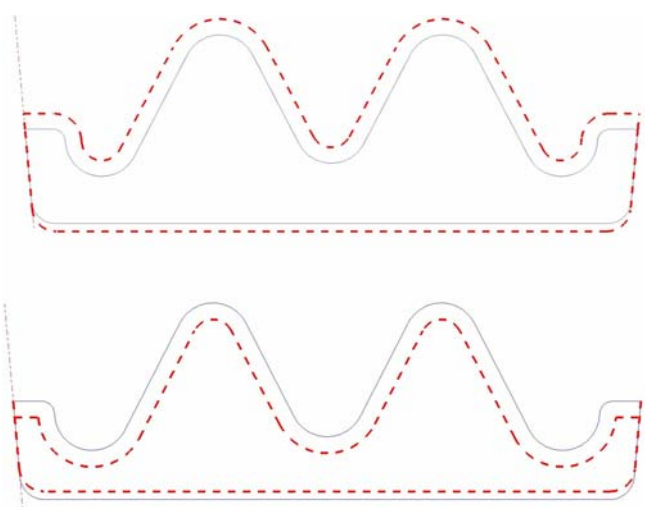

Figure 7 Range of Minimum and Maximum Shape Variation

A single variable GPO1 (gasket profile offset value) can describe the gasket profile offset value from the nominal shape. It was assumed that the gasket profile offset variable exhibits variation with a truncated normal distribution of mean value μ_{GPO1} = 0.0 in., a standard deviation σ_{GPO1} = 0.00052 in, and a range of values that can vary from -0.004 in. to 0.004 in. The groove depth in which the lower gasket is resting is considered as a random a design variable, GGD2 (lower gasket groove depth). It was assumed that the GGD2 variable exhibits variation with a truncated normal distribution of mean value μ_{GGD2} = 0.024 in., a standard deviation σ_{GGD2} = 0.00049 in., and a range of values that can vary from 0.022 in. to 0.026 in. The groove depth in which the upper gasket is resting is also considered as a random design variable, PGD3 (upper gasket groove depth). It was assumed that the PGD3 variable exhibits variation with a truncated normal distribution of mean value μ_{GGD2} = 0.010 in., a standard deviation σ_{GGD2} = 0.00049 in., and a range of values that can vary from 0.008 in. to 0.012 in. The interface gap between the bipolar plates is the fourth random design variable considered, IG4 (interface gap between the bipolar plates). It was assumed that the IG4 variable exhibits uniform random distribution with a range of values from 0 to 0.002 in. Table 1 shows the nominal value, the standard deviation, the upper specification limit (USL) and the LSL of all four random input variables. Figure 8 shows the probability density functions of all random input variables.

The target value for the gasket force is 18 lb/in, the LSL (i.e., the minimum force required for sufficient sealing) is 5 lb/in, and the USL (i.e.,, the maximum force that results in sufficient sealing and does not break the plate) is 30 lb/in. A probabilistic analysis was performed to assess the impact of this shape variation, the material properties, and the initial gap on the gasket reaction forces.

Table 1 Range of Random Design Variables

Design Variable	Nominal Value	Standard Deviation	LSL	USL
Gasket profile	0.000	0.00052	-0.004	0.004
Gasket groove depth	0.024	0.00049	0.022	0.026
Recessed pocket groove depth	0.010	0.00049	0.008	0.012
Interface gap	0.000	-	0.000	0.002

A central composite sampling technique is used to establish the combination of variable "experiments" that are used in the FEA analyses. The CAD-FEA integration enables the automatic generation of the geometries and their corresponding meshes. The gasket force is determined for each one of the experiments. A response surface function for the gasket force is computed as a function of all the design variables. If the "goodness" of the fit is acceptable, 10,000 random values for each design variable are generated using a Latin - Hypercube sampling technique. Figure 9 shows top and isometric views of a scatter plot of the Latin - Hypercube sampling of some random input variables. On the top and right-hand side of the 2-D scatter plot the corresponding probability density functions are shown. The 3-D scatter plot shows the Latin - Hypercube sampling of three random input variables.

Using the gasket force response surface function, 10,000 values of the gasket force are computed. In order to establish the robustness of the design, the mean value and the standard deviation of the gasket force are then computed and compared to the USL and LSL, and the "sigma-quality level" is determined. Figure 10 shows the workflow diagram used for the robust design process.

Figure 11 shows a histogram of the probability density of the gasket reaction force per unit length. Although all input parameters exhibit variation with normal or uniform distributions, the output parameter exhibits a high degree of asymmetry of its distribution around the mean value. The distance of the mean to the USL, measured in standard deviation units, is about 5.3 σ. The distance of the mean to the LSL is about 4.5 σ. Therefore, the sigma-quality level for this gasket design is the minimum value of the two distances, 4.5 σ.

CONCLUSIONS

Comparison of Mooney-Rivlin and Arruda-Boyce hyperelastic material models shows no difference in the deflected shape and similar load-gap curves. A 6.4% difference on the reaction force at 11.5 mils gap was observed. The reaction at 11.5 mils gap is 17.49 lb/in with the Mooney-Rivlin Material Model and 16.37 lb/in with the Arruda-Boyce Material Model. Figure 6 shows the load deflection curves for the Mooney-Rivlin and Arruda-Boyce material models. The Arruda-Boyce model is recommended for very large, tensile strains greater than 200%.

One of the major technical barriers in commercialization of fuel cells is the sealing of all gases and fluids between the bipolar and end plates. Currently the sealing is achieved with gaskets and grooves on the plates. This research effort provides a technique that can evaluate and improve the robustness of the sealing by optimizing the gasket shape and the groove depths.

The shape and size of the gasket's cross section that provided the desired sealing force were identified. The gasket design meets all requirements and is acceptable for the sealing system of the fuel cell plate design.

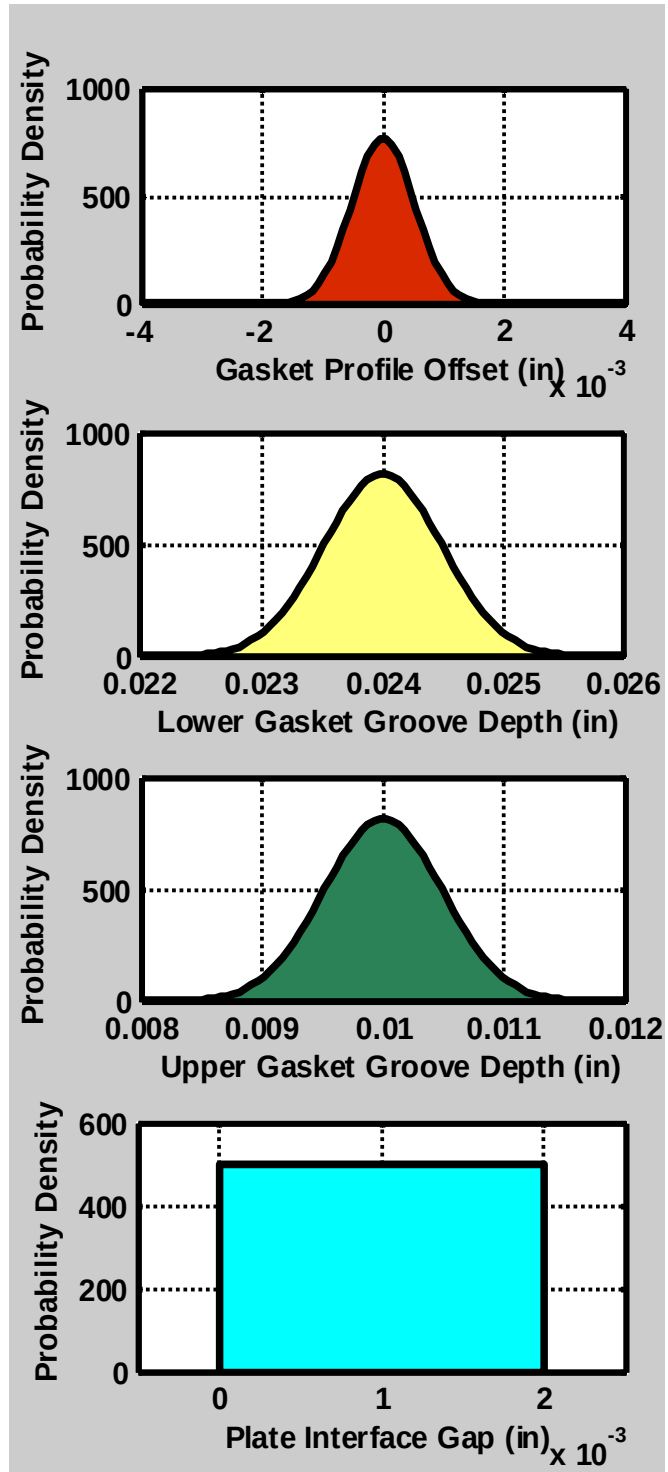

Figure 8 Probability Density Functions of Random Input Variables

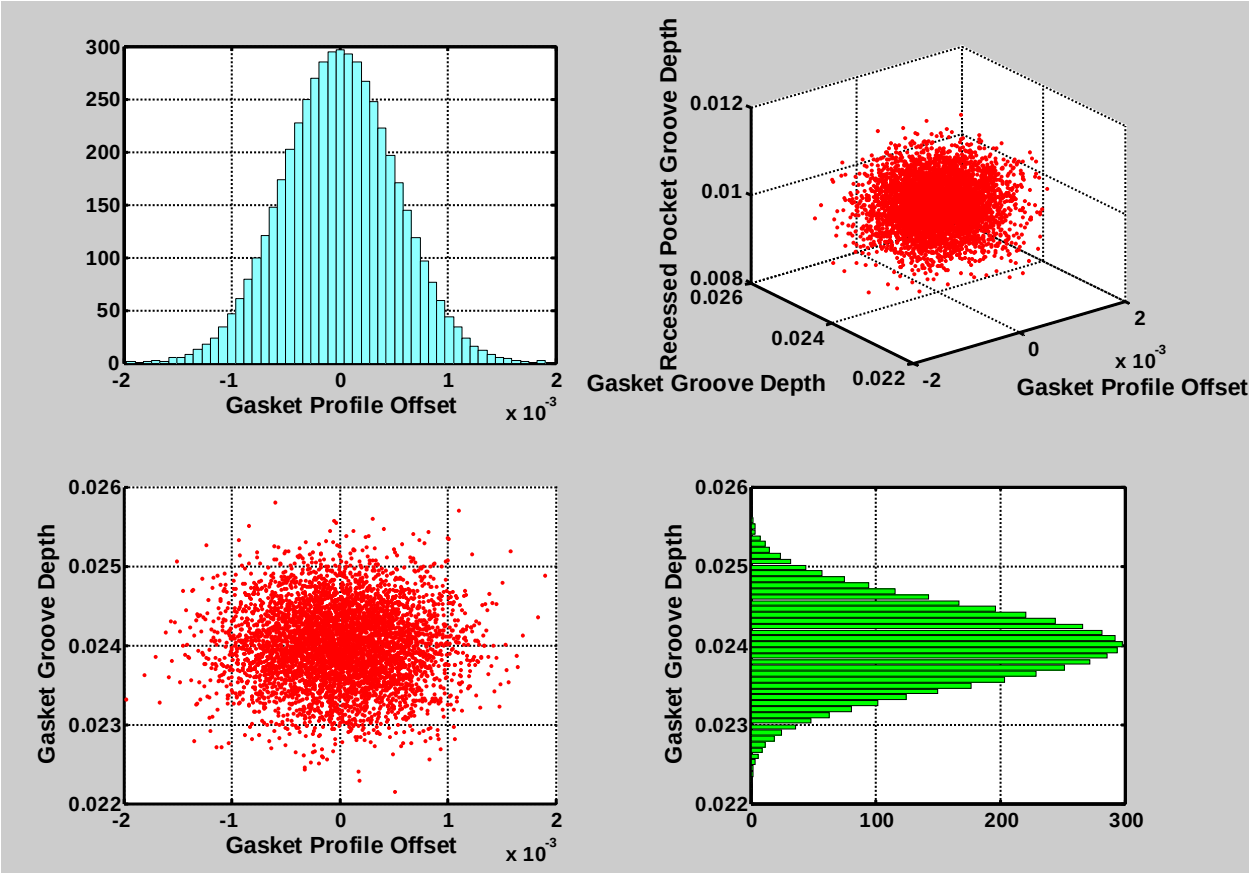

Figure 9 Top and Isometric Views of a Scatter Plot of the Latin - Hypercube Sampling of Three Random Input Variables.

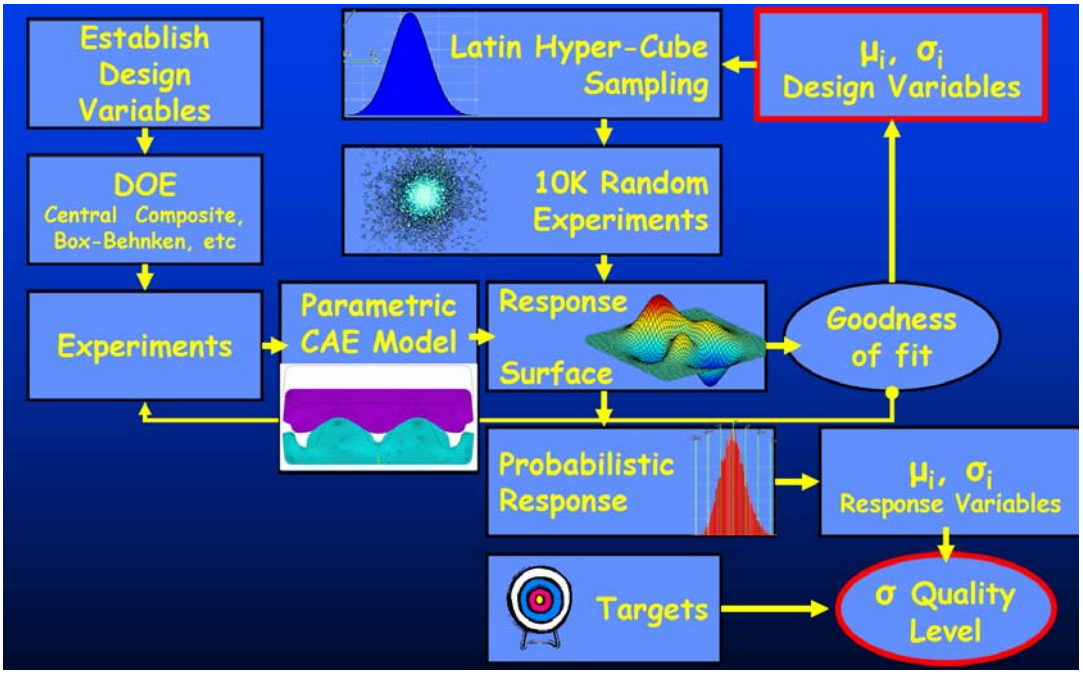

Figure 10 Workflow Diagram for Robust Design

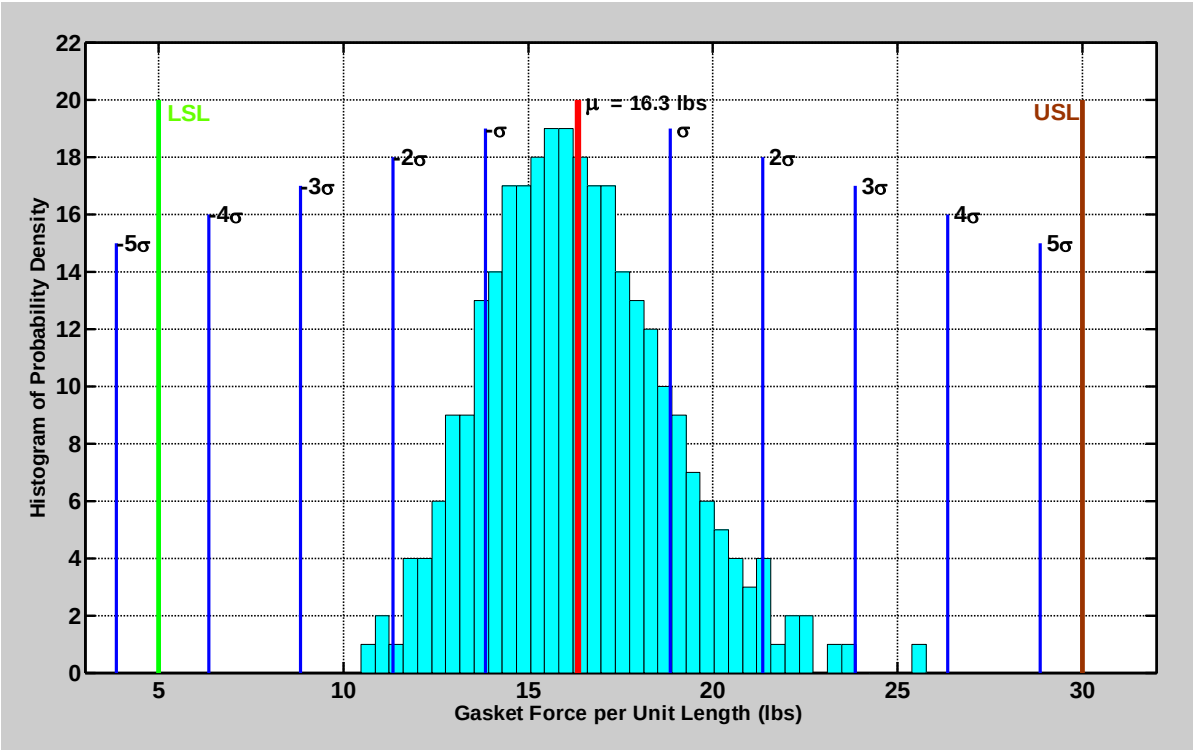

Figure 11 Histogram of Reaction Force Probability Density

ACKNOWLEDGMENTS

This research effort was funded by the U.S. Department of Energy, Office of Hydrogen Fuel Cells and Infrastructure Technologies. The authors would like to express their appreciation to Kathi Epping and Nancy Gardner of the Hydrogen, Fuel Cells & Infrastructure Technologies Program; Terry Penney of the National Renewable Energy Laboratory,; and to William Ernst of Plug Power, Inc. for their support of this project.

REFERENCES

1. Arruda, E.M. and Boyce, M.C. “A Three-Dimensional Constitutive Model for the Large Stretch Behavior of Rubber Elastic Materials,” J. Mech. Phys. Solids, 41. (1993) 389-412.
2. ANSYS Inc. “Probabilistic Design Techniques,” Advanced Analysis Techniques Guide, August 2002.
3. ANSYS Inc. “Viscoelastic Material Curve Fitting,” Structural Analysis Guide, Release 10.0.
4. Schmidt, R. and Launsby S. Understanding Industrial Designed Experiments, 4th edition, Air Academy Press, 2000.
5. Vlahinos A. and Kelkar S. "Body-in-White Weight Reduction via Probabilistic Modeling of Manufacturing Variations," 2001 International Body Engineering Conference, SAE paper # 2001-01-3044, Detroit, MI, October 2001.
6. Vlahinos A. and Kelkar S. "Designing For Six-Sigma Quality with Robust Optimization using CAE," 2002 International Body Engineering Conference, SAE paper # 2002-01-2017, Paris, France, July 2002
7. Vlahinos, A., Penney T., and Kelkar S. "Engineering Quality into Digital Functional Vehicles," proceedings of IDPS2002, 2002 Daratech Intelligent Digital Prototyping Strategies Conference, Detroit, MI, June 2002
8. Vlahinos A., Kelly K., Pesaran A., and Penney T., "Empowering Engineers to Generate Six-Sigma Quality Designs," proceedings of First Annual Quality Paper Symposium, American Society for Quality, Automotive Division, Livonia, MI, February 200.
9. Vlahinos, A. “Design Optimization for Six-Sigma Quality,” Simulation versus Reality Seminar, NAFEMS, International Association for the Engineering Analysis Community, Dearborn, MI, July 2005.
10. Vlahinos, A. and Penney T. “Design Optimization for Six-Sigma Quality,” Ninth International Conference on Computer Aided Optimum Design in Engineering, Skiathos, Greece, May 2005.